RESEARCH ARTICLE - SOLID EARTH SCIENCES

CrossMark

Characterization of site conditions for selected seismic stations in eastern part of Romania

B. Grecu[1] · B. Zaharia[1] · M. Diaconescu[1] · A. Bala[1] · E. Nastase[1] · E. Constantinescu[1] · D. Tataru[1]

Abstract

Strong motion data are essential for seismic hazard assessment. To correctly understand and use this kind of data is necessary to have a good knowledge of local site conditions. Romania has one of the largest strong motion networks in Europe with 134 real-time stations. In this work, we aim to do a comprehensive site characterization for eight of these stations located in the eastern part of Romania. We make use of a various seismological dataset and we perform ambient noise and earthquake-based investigations to estimate the background noise level, the resonance frequencies and amplification of each site. We also derive the Vs_{30} parameter from the surface shear-wave velocity profiles obtained through the inversion of the Rayleigh waves recorded in active seismic measurements. Our analyses indicate similar results for seven stations: high noise levels for frequencies larger than 1 Hz, well defined fundamental resonance at low frequencies (0.15–0.29 Hz), moderate amplification levels (up to 4 units) for frequencies between 0.15 and 5–7 Hz and same soil class (type C) according to the estimated Vs_{30} and Eurocode 8. In contrast, the eighth station for which the soil class is evaluated of type B exhibits a very good noise level for a wide range of frequencies (0.01–20 Hz), a broader fundamental resonance at high frequencies ($\sim$ 8 Hz) and a flat amplification curve between 0.1 and 3–4 Hz.

Keywords Ambient seismic noise · Resonance frequency · Soil amplification · Rayleigh waves · Vs_{30}

Introduction

Romania is considered one of the most vulnerable countries in Europe at strong earthquakes. Its seismicity is dominated by the Vrancea intermediate-depth earthquakes. These earthquakes are generated within a narrow focal volume located beneath the region of the maximum curvature of the Eastern Carpathians, at depths between 60 and approximately 200 km. The strong earthquakes occurred in this area produce significant damage over an extended area elongated in the NE–SW direction, predominantly in the extra-Carpathian area. The crustal seismicity is not as substantial as the subcrustal one, and it is generated in several seismogenic zones across the country (Radulian et al. 2000).

In the last four decades, 28 moderate-to-strong earthquakes with magnitudes (M_w) between 5.0 and 7.4

occurred on the Romanian territory, of which only 5 in the crustal domain (from Romanian catalog ROMPLUS— www.infp.ro). To monitor and adequately record the strong ground motion during such kind of events, the National Institute for Earth Physics (NIEP) has developed the Romanian Strong-Motion Network (RSMN). At present, RSMN consists of 134 stations installed in different environments (free-field, buildings, vaults) all over the country. The RSMN stations record the ground motion continuously and using a real-time communication system the data is sent to the Romanian National Data Center (RONDC) in Magurele, Romania.

Strong motion data are very important for seismic hazard studies as they are used as input for the derivation of the ground-motion prediction equations (GMPEs). The quality and the proper understanding of the recorded strong ground motion depend on the performance of the seismic equipment as well as on a complete characterization of the site. This characterization includes, besides the geological and technical information about the location and equipment, a good knowledge of the local site conditions as they

✉ B. Grecu
bgrecu@infp.ro

[1] National Institute for Earth Physics, Măgurele, Romania

could change the frequency content of the ground motion, amplify it and extend its duration.

In this paper, we investigate the site conditions at 8 RSMN stations located in the eastern part of Romania (Fig. 1). The motivation of the selection of the stations is twofold. Firstly, they cover now an area which was poorly monitored before 2013 when an unusual seismic swarm occurred NW to the city of Galati. Secondly, the distribution of the accelerations recorded by RSMN stations shows, after each significant earthquake with magnitude $M_L \geq 4.0$, higher values for most of the stations used in the study and located in the vicinity of the Galati city than for almost all other stations. This behavior is seen in Fig. 2 which portrays the distribution of the maximum accelerations recorded by RSMN stations during the 2nd of August 2017 Vrancea earthquake ($M_L = 4.9$, $H = 133$ km) and the 16th of August 2017 Galati earthquake ($M_L = 4.0$, $H = 11$ km).

The investigations we performed in this study include characterization of the noise level at the stations, estimation of the fundamental characteristics of the ground motion using noise and earthquake data and determination of the shallow velocity structure and the Vs_{30} parameter.

Seismotectonic setting

The Eastern part of Romania has a particular tectonic environment which consists of several major tectonic units (East-European Platform, Scythian Platform, Moesian Platform and North Dobrogea tectonic unit) and major

faults which bound these tectonic units: Peceneaga–Camena fault—the tectonic limit between Moesian Platform and North Dobrogea, Sf. Gheorghe fault—the boundary between North Dobrogea and Scythian Platform and Trotuş fault—the limit between Scythian Platform and East European Platform. Three of the investigated sites (Scanteiesti (SCTR), Tatarca (TATR) and Vladesti (VLDR)) are located on Scythian Platform while all other stations are on North Dobrogean Promontory (Fig. 3). The internal structure of the Scythian platform is less known than that of the East-European Platform (Matenco et al. 2003), due to thicker Tertiary sediments in the Bârlad Depression and to underthrusting below the Eastern Carpathians nappe pile. Carcaliu (CFR) site is located on the Macin nappe area of the North Dobrogean tectonic unit. The North Dobrogea tectonic unit is situated between the Scythian and Moesian Platforms, and it is composed of a complex deformed Hercynian basement and a Triassic–Cretaceous sedimentary cover, unequally developed (Ionesi 1989). West of the Danube, the basement and Mesozoic sediments are covered by a succession of Tertiary deposits, forming the North Dobrogea Promontory.

Before 2013, the seismic activity in the area was characterized by the occurrence of dispersed earthquakes of small-to-moderate size, the largest event with a moment magnitude of 4.2 being recorded on the 11th of September 1980 (ROMPLUS catalog Oncescu et al. 1999). In August 2013, an uncommon seismic swarm started in the Galati area. The activity during the swarm period was characterized by a large number of events (940) with local magnitudes from 0.1 to 4.0 occurred in the time interval from

Fig. 1 Map with the location of the investigated sites plotted together with the seismicity (red stars—intermediate-depth earthquakes, yellow circles—crustal events)
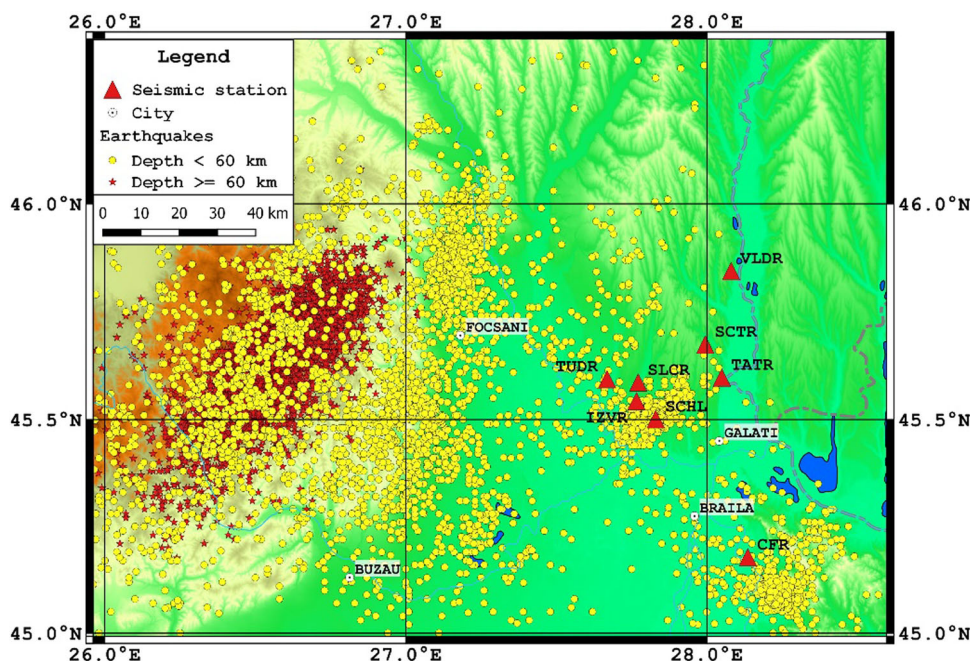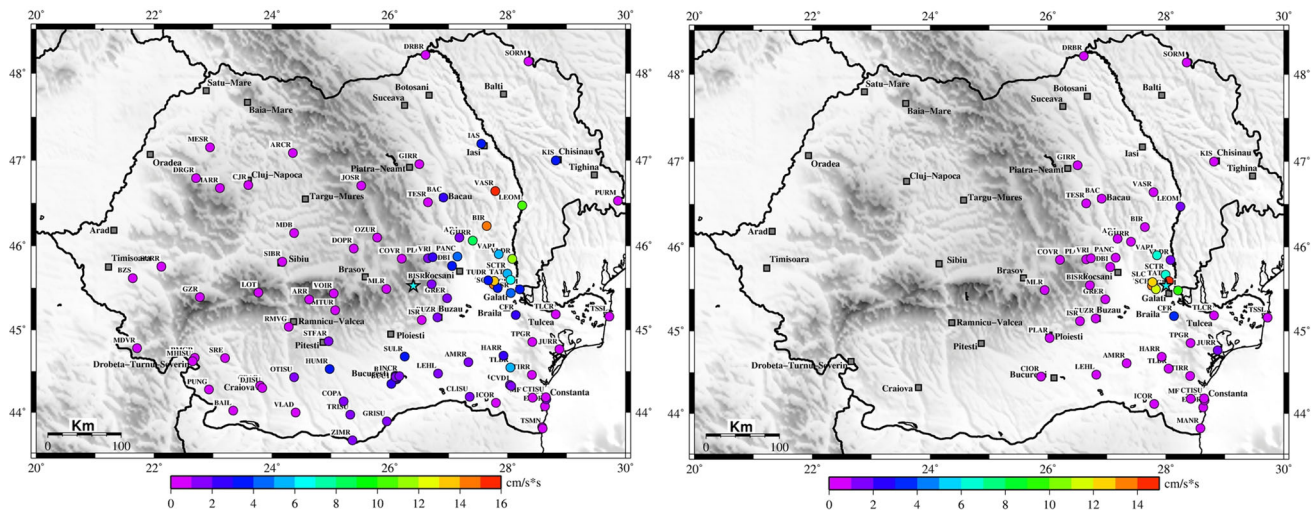
Fig. 2 The distribution of the maximum acceleration recorded during two local events: (left) the 2nd of August 2017 Vrancea intermediate-depth earthquake (M_L = 4.9) and (right) the 16th of August 2017 crustal earthquake (M_L = 4.0). Blue star—earthquakes epicenter
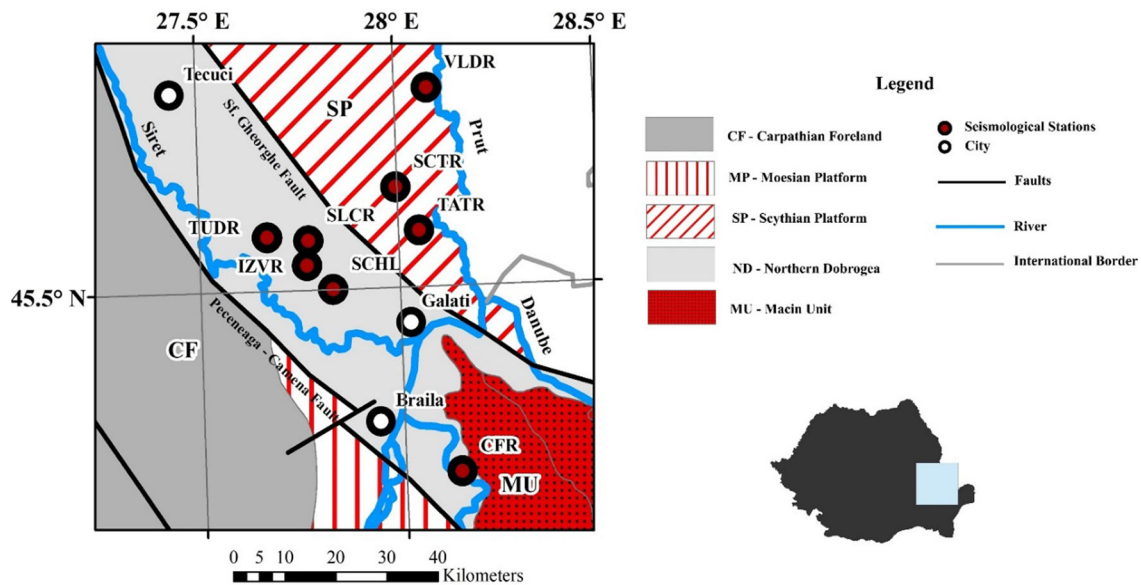

Fig. 3 Tectonic map of the investigated area (after Sandulescu 1984). Seismic stations are also depicted with red dots

15th August to 5th November (Popa et al. 2016). The earthquakes epicenters were located between the Sf. Gheorghe fault and Peceneaga–Camena crustal fault.

The region located to the SE of Galati city is characterized by the seismic activity clustered in the Predobrogean seismogenic zone (Radulian et al. 2000) and also by numerous artificial events generated in many quarries present in the area (Ghica et al. 2016).

Dataset description and investigations performed

The RSMN operated by NIEP in the study area was sparse before 2013, with only one station (CFR) existing to the SE of Galati city. The situation changed starting with spring 2013, when three more stations were deployed, one before and two during the Galati swarm. The network was upgraded with a new station in 2014 and two more in the middle of 2015 (Fig. 4). All sites are equipped with both broadband velocity sensors and accelerometers. The data

used in this study are of three types: seismic noise, earthquake and active seismic data.

Seismic noise data

We used the seismic noise data with two purposes: first, to characterize the noise level at the stations and second, to estimate the fundamental resonance frequency of the sites. In the first case, we assessed the level of seismic noise by computing the Probability Density Functions (PDFs) for a large number of Power Spectral Densities (PSDs) (McNamara and Buland 2004). Many studies took advantage of the PDF versatility and used it to evaluate seismic stations performance and compute the noise level at the seismic sites (McNamara and Buland 2004; Diaz et al. 2010; Evangelidis and Melis 2012; Grecu et al. 2012). For this analysis, we used the entire dataset available at each station location.

In the late 80's and the 90's, numerous studies focused on local site investigations and used the ratio between the horizontal and vertical spectral components of seismic noise (hereinafter HVNR—"Horizontal to Vertical Noise Ratio") to characterize the seismic response of the subsoil. The peak of the HVNR curve is often associated with the fundamental resonance frequency of the site, and its amplitude and sharpness are related to the shear-wave impedance contrast in the subsoil (Nakamura 1989; Bard 1999). The HVNR analysis was performed at each station using 10 days of continuous data, recorded from 1st to 10th of January 2017 (the period was randomly selected) using the velocity sensors. The long duration of the recordings allowed us to use windows of 100 s length and, therefore, to go in our investigations to lower frequencies (up to 0.1 Hz) (SESAME project-2005). We used an automatic procedure based on an anti-triggering algorithm to avoid transient noise and to select stationary time windows. Figure 4 shows the number of windows used in HVRN noise analysis for each station. The data selection and processing were done using Geopsy software (www.geopsy.org).

Earthquake data

In this study, we used earthquake data to obtain information on the resonance frequencies (Lermo and Chávez-García 1993; Field and Jacobs 1995) as well as on local amplification of the investigated sites. The used method (hereinafter HVSR—"Horizontal to Spectral Vertical Ratio") is very similar to the HVNR method used for noise data. Figure 5 portrays the methodology we followed. The HVSR analyses were performed on 60 s time windows, starting from the P-waves onset. This window length allowed us to include the S-wave train which usually contains the most energetic part of the record as well as the coda wave of which spectral shape depends only on the local heterogeneities in the crust (Philips and Aki 1986). Grecu et al. (2011) used both S-wave and coda wave to investigate the site effects at several stations installed in eastern part of Romania during a temporary seismic experiment. They found no significant differences regarding the resonant frequencies of the HVSRs computed for the two types of waves, while the level of the amplification for S-wave is slightly higher than for coda waves.

The HVSR analysis was performed using earthquake data recorded by the strong motion sensor located at each station. We used 54 local earthquakes with $M_w \geq 4.0$ (from Romanian ROMPLUS catalog) recorded between 2010 and 2017. Since the stations have been installed in various time periods and consequently have different recording periods, the number of earthquakes recorded is different from one station to another. In Fig. 4 are shown the number of earthquakes used in the HVSR analysis for each site.

Active seismic data

Active seismic measurements have been performed at all station sites, except for station Slobozia Conachi (SLCR) for which no seismic survey was possible. These measures aimed to record surface waves generated by an active source (sledgehammer) and invert their dispersive properties for the determination of the V_S vertical profile and, the Vs_{30} parameter. The dataset was acquired using a 3-C

Station code	Before 2013	2013	2014	2015	2016	2017	No. win.	No. eq.	Offset (m)
CFR		XXX					2258	54	44
IZVR		XXX					4479	18	63
SCHL		XXX					1030	21	63
SCTR		XXX					5331	13	45
SLCR		XXX					4524	12	-
TATR		XXX					2328	12	61
TUDR		XXX					2591	28	63
VLDR		XXX					1053	13	60

Fig. 4 The data availability, the number of windows (No. win.) and earthquakes (No. eq.) used for HVNR and HVSR analyses and the profile lengths (offset) for each station. With X is marked the period of the Galati swarm
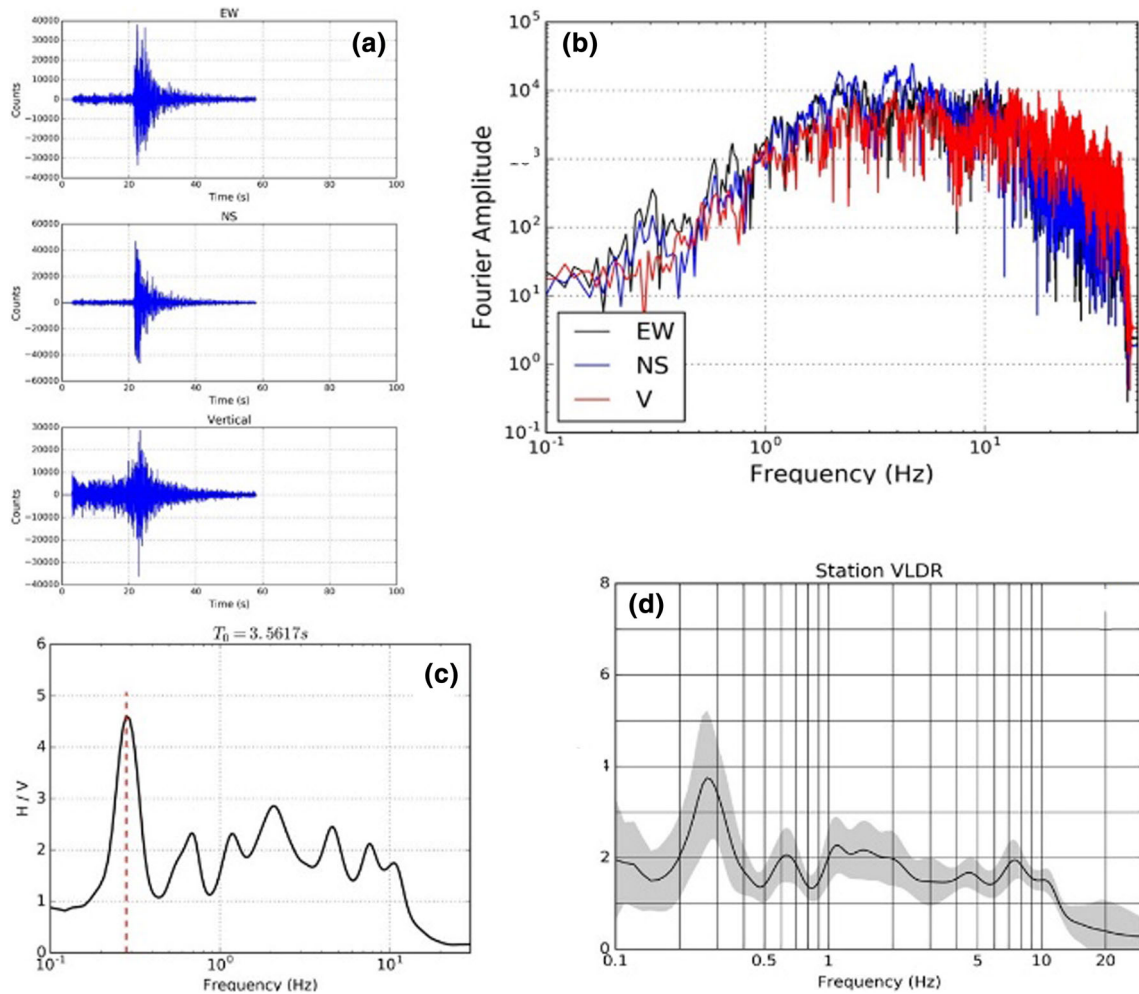
Fig. 5 The methodology used for estimating the local amplification at a given station: **a** selection of earthquake recordings and cut off of 60 s window length (the waveforms are from a subcrustal earthquake with $M_w = 4.6$ occurred in Vrancea area on 2nd of August 2017) **b** computation of the Fourier spectra for Z, NS and EW components for the selected earthquake **c** computation of the spectral ratio for the chosen earthquake by dividing the smoothed average spectrum of the horizontal components to the vertical one; the spectra are smoothed using the Konno and Ohmachi (1998) recording window ($b = 20$) and the horizontal average spectrum is computed as geometric mean of the two horizontal components (**d**) the HVSR curve obtained by averaging the results obtained for each event

geophone with a natural frequency of 2 Hz. The use of 3-C geophone allowed obtaining multichannel data consisting of vertical and radial components of Rayleigh waves (the geophone was oriented such that its horizontal NS axis was along the profile). No Love waves were used in the analysis since their recording requires a different setup for generating them (wooden beam and horizontal force) which was not available during the measurements. Because of logistic limitations, the maximum profile length (offset—the distance between the active source and the recording sensor) was 63 m. In Fig. 4 are shown the offsets of the surveys at each station. The profile length limits the maximum penetration depth to about two-third of the adopted offset if some conditions are met (Dal Moro 2014).

Each survey consisted of two sets of measurements. For each group, we generated four shots, and we stacked the
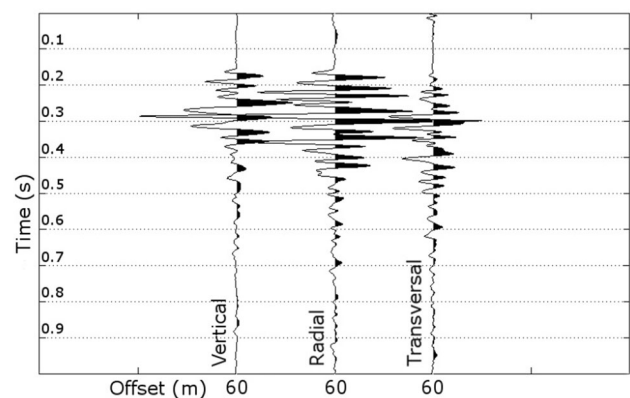

Fig. 6 Stacked traces obtained at station VLDR

resulting traces to attenuate the incoherent noise and obtain the final record. Figure 6 shows the stacked field data collected at station VLDR. In our analysis, we used the best measurements of the two sets.

The analysis of the surface waves (Rayleigh type) follows the approach described by Dal Moro (2014). In this method, the signals recorded in the field are transformed into the frequency–velocity domain to yield the velocity spectrum (VS) which is further used in an inversion procedure to retrieve the shallow velocity structure. The advantage of this method compared to classical one's lies in the manner the VS is used for the inversion. Thus, in this approach, the whole VS is used while in the traditional method the modal dispersion curves are picked subjectively by the user and used as input for the inversion.

Results

Background noise level

To estimate the background noise level at each station, we used the statistical mode of the PDF computed for the vertical component, as this curve corresponds to the highest probability noise level of a given site (McNamara and Buland, 2004). Figure 7a shows an example of the PDF computed for station CFR. The high-probability region corresponds to the power values associated with the background seismic noise. This domain is relatively close to the Peterson's (1993) new low noise model (NLNM) for periods between 0.1 s and 179 s, indicating thus a good background noise level for the station. An increase of almost 30 dB of the noise level is observed for periods smaller than 0.1 s. The noise level at these periods is strongly affected by anthropogenic noise sources, which in this case, are related to the human activities carried out in a rural household located very close (about 15–20 m) to the station. Figure 7b portrays the stations PDF mode noise levels plotted together with three reference noise models: the Peterson's New High Noise Model (NHNM), New Low Noise Model (NLNM) and the Romanian Noise Model (RONM) (Grecu et al. 2017). All stations show high noise levels, very close to or even exceeding the NHNM, for periods lower than 1 s and larger than 20 s, except for CFR site. The variation of the noise levels is much smaller in the microseismic band (2–20 s) where noise levels are related mainly to the energy released by oceanic waves (Stutzmann et al. 2009). The higher noise levels observed for IZVR, SCHL, SCTR, SLCR, TATR and TUDR sites at small periods (< 1 s) are related to the location of these stations. They are installed on soft and thick sediments within villages or within a monastery (TUDR station) where human activities are more significant than for CFR station. At periods larger than 20 s, the difference between the noise level at CFR and the others is given mainly by the instrumentation and the proper thermal isolation of the sensor of station CFR.

Site condition analysis

Detailed analysis of the HVNR results obtained at seismic stations indicates two types of HVNR curves: one dominated by a clear peak at low frequencies corresponding to the fundamental resonance peak and one with a broad peak at high frequencies. The former is characteristic for seven stations (IZVR, SCHL, SCTR, SLCR, TATR, TUDR, VLDR) while the latter is observed at just one site (CFR) (Fig. 8). In the first case, the frequency of the fundamental resonance peak increases from 0.15 Hz at TUDR station towards 0.29 Hz at TATR station while its amplitude varies from 3.9 observed at station SCHL to 7 at station VLDR. A secondary peak, much broader, is also seen at
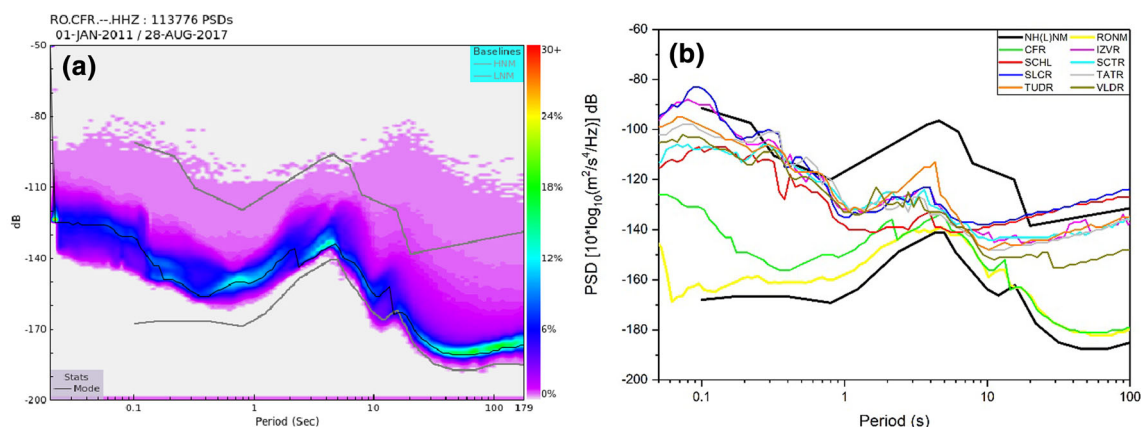

Fig. 7 **a** PDF for station CFR, the black line being the mode of the PDF and the gray lines correspond to the NLNM and NHNM curves **b** stations mode plotted together with three reference models: NHNM, NLNM and RONM
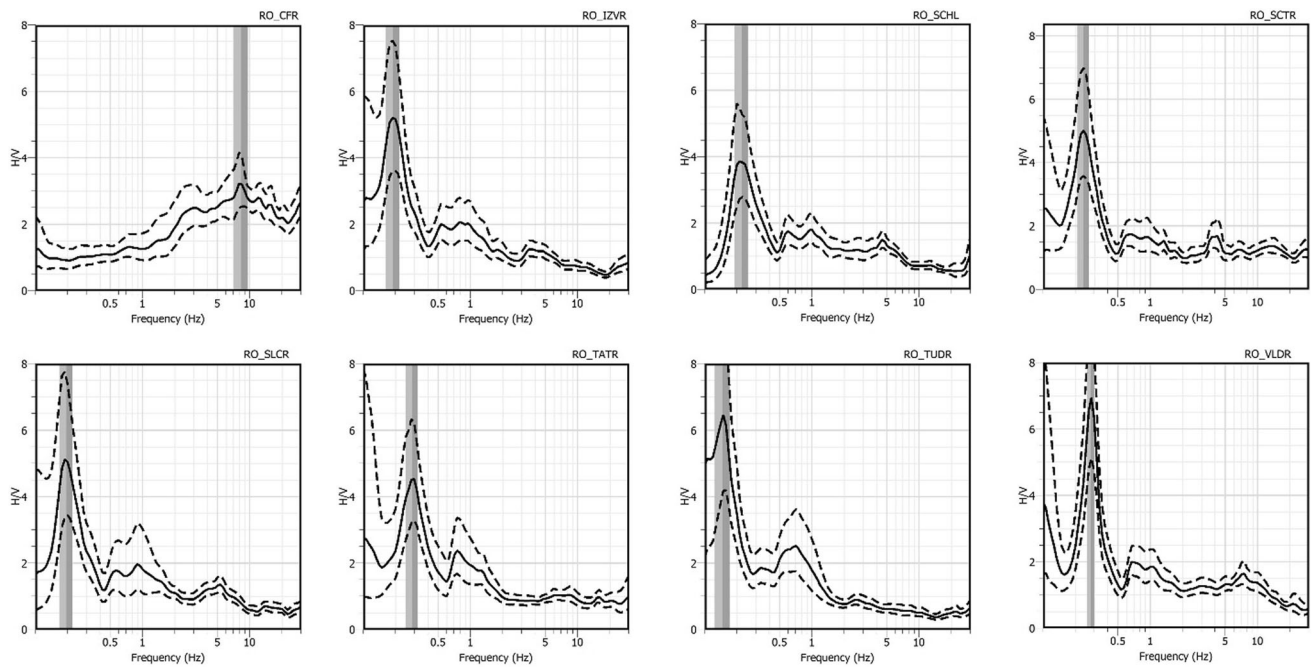
Fig. 8 The HVNR results for all stations

frequencies between 0.5 and 1 Hz. This peak is well defined and its amplitude exceeds 2 only for stations TATR and TUDR. For station CFR, the HVNR curve shows nearly flat amplitude below 2 for frequencies smaller than 2 Hz. For frequencies larger than 2 Hz, an increase in the amplitude of the HVNR curve is observed and its maximum of 3.2 units is reached at about 8 Hz. The resonance frequency of each site depends on the nature and thickness of the layers' underneath. All the stations located to the N and NE of Galati city are installed on relatively thick sediments. For example, TUDR station is located on the external margin of Carpathian foredeep, on 3 km depth of sedimentary rocks; the first 1.3 km are soft rocks of Neogene formations. Underneath lies the basement of Pre-Dobrogean depression with V_S velocities of about 3300 m/s (Raileanu, Annual report 2006).

This fact is reflected in the low-frequency fundamental resonance peak of the HVNR curve. The difference in frequencies of the fundamental resonance peak observed at these stations is related to the variations in the sediment thickness (Ibs-von Seht and Wohlenberg 1999) beneath these stations.

For station CFR, which is located on North Dobrogean Orogen, on old rocks of Paleozoic origin, the Paleozoic sediments overlie a Hercynian basement consisting of crystalline schists of Proterozoic age (Balan et al. 2014). The increase at high frequencies of the HVNR amplitude at CFR station can be related to the presence of a thin weathered soil of just a few meters, overlying the hard rock.

The HVNR amplitude azimuthal variations were also investigated (Fig. 9). For all the stations, except CFR station, the amplitude corresponding to the low fundamental frequency varies very little with the azimuth. On the contrary, the HVNR amplitude obtained for station CFR shows a high dependency on the azimuth at frequencies between 8 and 9 Hz. Large azimuthal variations could indicate either an interaction with a nearby structure or complex site effects (topographical irregularities, rock degradation), the latter being the most likely for station CFR.

Figure 10 shows the HVSR curves obtained using earthquake data. On the one hand, the results confirm to some extent the findings obtained from noise data, and on the other hand, they show some features that are not present in HVNR curves.

For all stations, the fundamental resonance frequency highlighted by the HVNR technique is also present in the HVSR curves, but only for stations CFR, IZVR, SCHL, SCTR and VLDR its amplitude is larger or at least similar with the other resonances. The resonance peak observed in the frequency domain 0.5–1 Hz has comparable amplitude with the one identified in HVNR curves, except for station TATR for which a value of 3 is reached. Another similarity between HVNR and HVSR curves is well recognized for station CFR. Both spectral ratios are relatively flat for a wide frequency band (from 0.1 to 2 Hz) and show amplitudes up to 3, for frequencies between 5 and 10 Hz. The main difference between the HVNR and HVSR curves is observed in the frequency band 1–7 Hz. In this range, all
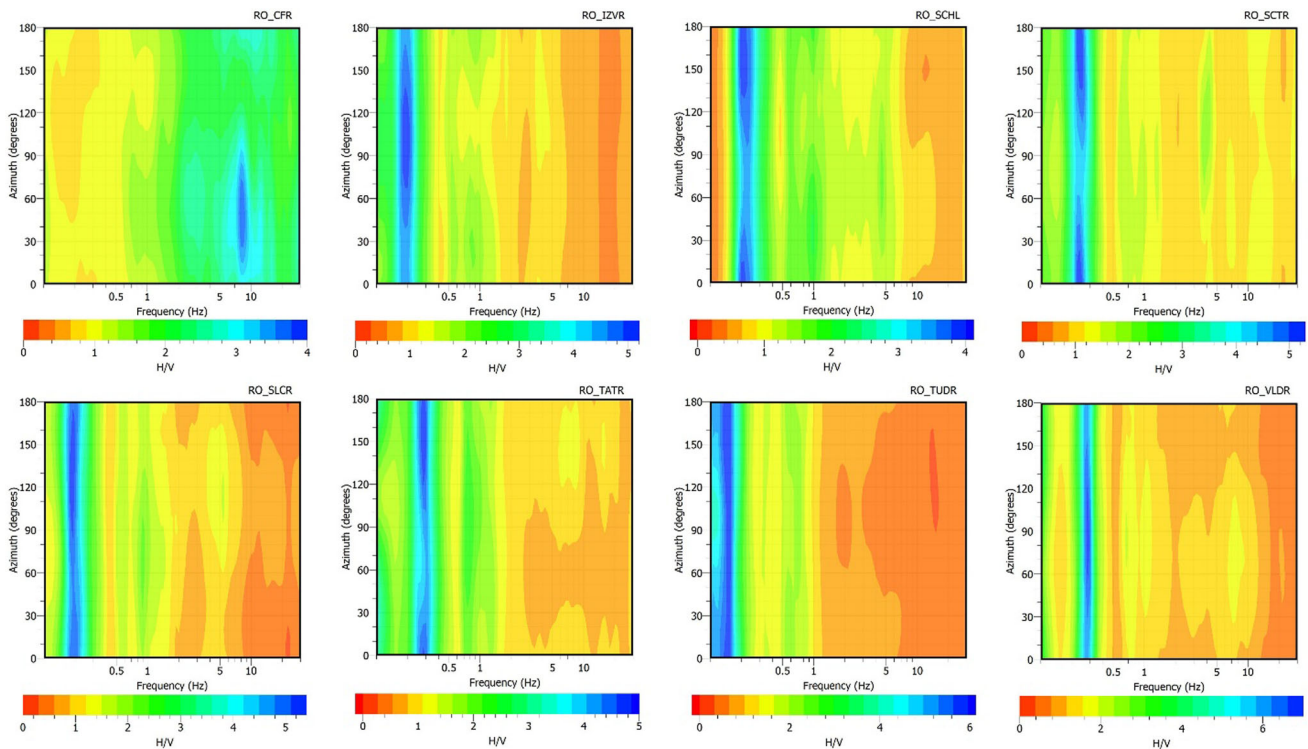
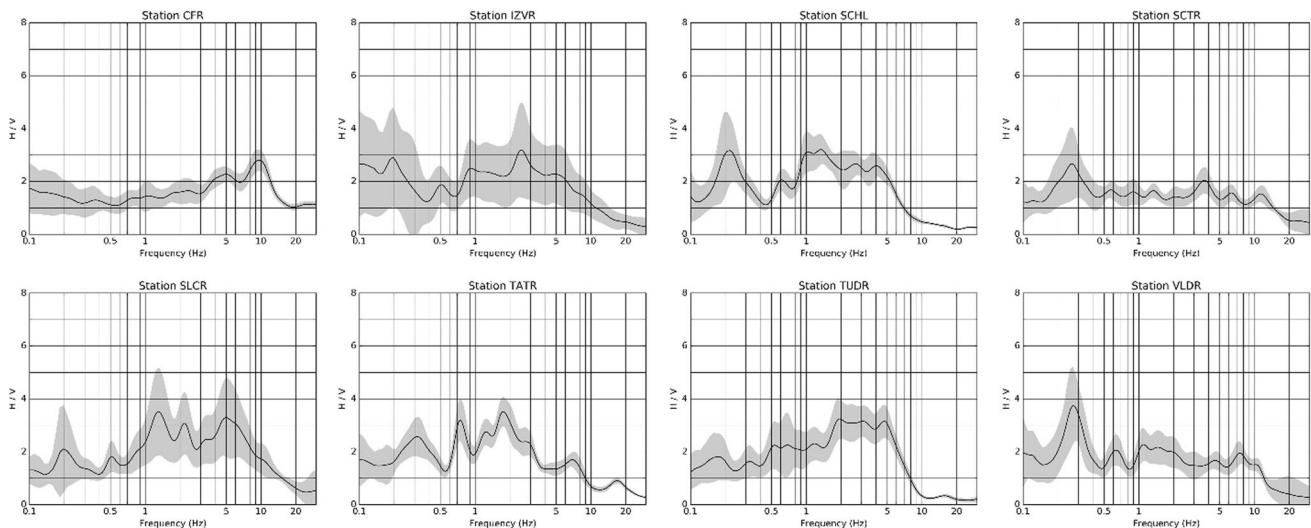**Fig. 9** The variation of the HVNR amplitude with azimuth

Fig. 10 HVSR results for all stations

the stations located in the Galati area exhibit amplifications around 3.

Shallow velocity structure, Vs$_{30}$

The derivation of the shallow velocity structure underneath each site and estimation of Vs$_{30}$ for soil class evaluation was done using the tools of the HoliSurface software

(www.winmasw.com) and consisted mainly of three steps. In the first step, we transformed the stacked trace from the offset-time domain into the frequency-velocity domain, and we obtained the VS (Fig. 11a). Next, we used different test velocity models to compute several synthetic VSs. The software uses the modal summation technique to calculate the synthetics. In this step, we modified the parameters of the test velocity models (shear-wave velocity and depth)
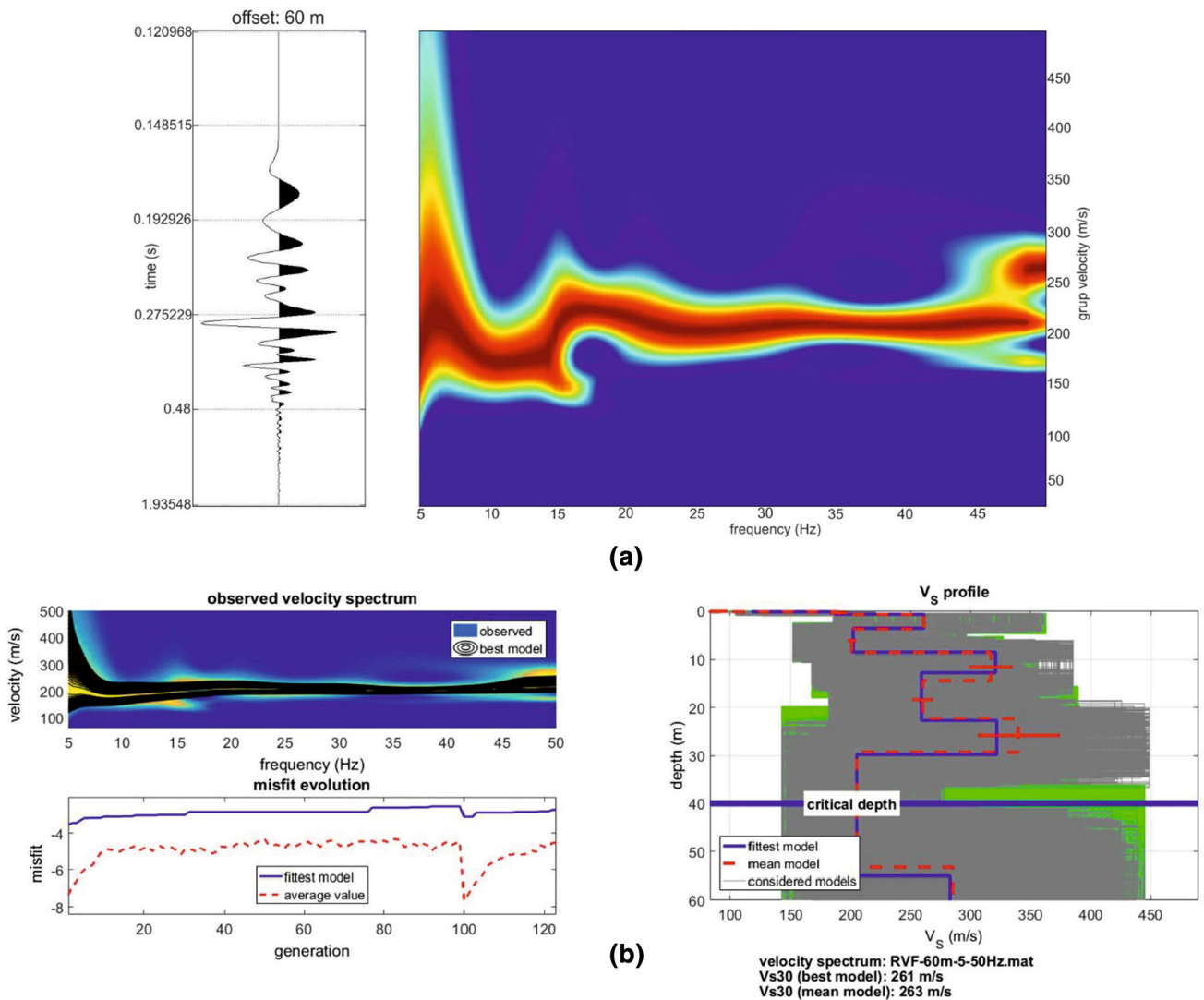
(a)

(b)

velocity spectrum: RVF-60m-5-50Hz.mat
Vs30 (best model): 261 m/s
Vs30 (mean model): 263 m/s

Fig. 11 a The radial component obtained in the field at station VLDR after the summation procedure and its observed velocity spectrum (**b**) inversion results (upper left—the fit between the VS of the best model and the observed FVS, right—velocity profiles for the best and mean models with blue line and red dotted line, respectively, and all models with gray lines) and the misfit evolution during the inversion procedure (lower left)

until we reached an acceptable fit between the observed VS and the computed VS. Then, we chose the final test model as starting model in the inversion performed in the last step. The inversion scheme is based on a genetic algorithm (Dal Moro et al. 2007) and, in summary, tries to minimize the misfit between the observed VS and the computed VS by changing the starting model iteratively. Finally, the Vs_{30} is automatically calculated from the derived shear-wave profile, and the soil class is ascertained. This final step is exemplified in Fig. 11b for station VLDR. The figure portrays the fit between the best FVS and observed FVS (upper left panel), the misfit evolution (lower left panel) and the retrieved Vs profiles for the best and mean model (right panel). In the case of station VLDR, the Vs_{30} is 261 and

263 m/s for the best model and mean model, respectively, while the soil class according to EC8 is C.

Since in our study we considered only vertical-impact source we could perform the inversion only for the vertical and radial components of the Rayleigh wave. In Fig. 12 are compared the shear-wave velocity profiles derived from the inversion of the vertical and radial traces recorded at station TATR. Some differences can be observed between the two profiles. These differences are also passed to the Vs_{30} values estimated from the two datasets. The Vs_{30} derived from the vertical component of the Rayleigh wave has a value of 267 m/s while for the radial component is 239 m/s. However, the differences are not large and the soil classification is C in both cases.
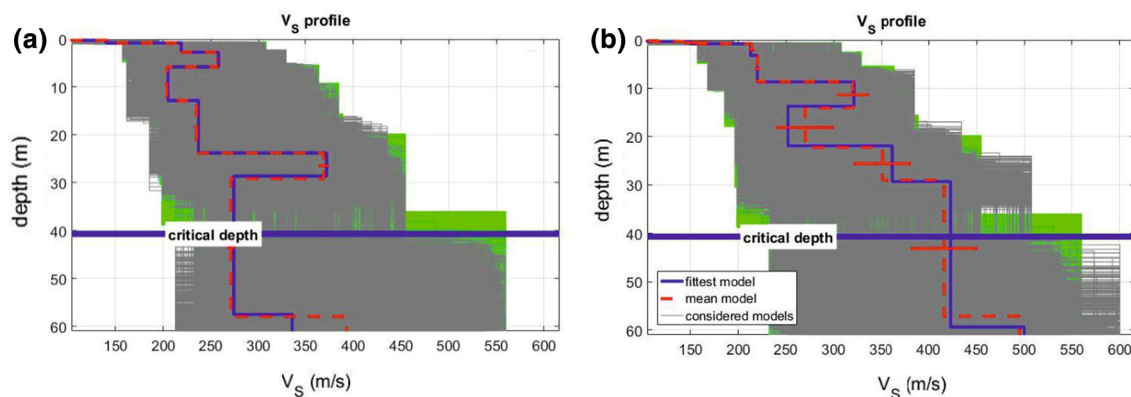
Fig. 12 V_s profiles obtained from the inversion of the vertical (**a**) and radial (**b**) component of Rayleigh wave (blue and red lines represent the best and mean models, respectively; gray lines—all models)

Considering both components (vertical and radial) of the Rayleigh wave recorded at each station, we have also performed a joint analysis of the two datasets. This common inversion has the advantage of better constraining the solution by excluding the models that cannot explain both datasets. The joint inversion has a different way of computing and treating the misfits. In this case, the misfits of each dataset are kept separately, and a ranking procedure evaluates their values based on the Pareto dominance criterion (Dal Moro and Ferigo 2011). Finally, the Pareto bi-objective space allows to choose the best model, and the symmetry of the Pareto front models constitutes an index of the general consistency of the whole inversion process (Dal Moro (2008); Dal Moro and Ferigo (2011)). The results using the joint inversion, for the TATR site, can be seen in Fig. 13. In this case, the computed value for Vs$_{30}$ is 263 m/s. If we compare this value with those obtained from the inversion of just one dataset we notice that the differences are relatively small and the soil class for TATR site is still C. Table 1 gives a summary of the Vs$_{30}$ values obtained from the inversion of the Rayleigh wave.

Discussion and concluding remarks

In this study, we applied different techniques and used various datasets (noise, earthquake and seismic active data) with the aim of investigating the site conditions at eight permanent stations of the Romanian Strong Motion Network.

The noise data were used with two purposes: first, to determine the noise level at the stations and second, to estimate the fundamental resonance frequency of each site. The investigation of the noise level at individual stations, which was performed using the PDFs, outlined only one station (CFR—located on North Dobrogean orogen) with a good noise level over a wide period domain (0.05–100 s). The other seven stations (IZVR, SCHL, SCTR, SLCR, TATR,

TUDR, VLDR) show noise levels much higher, in particular for periods smaller than 1 s and periods larger than 10 s. In the first case, the noise is generated mainly by anthropic activities, and the noise level depends on the sources and the distance to the sources. All seven stations are installed within villages, and the different human activities in each village are reflected in different noise levels. It has been shown (Grecu et al. 2012, 2016) that the noise level in the microseismic domain (2–10 s) depends, among other things, on the thickness of the sediments underneath the station. All seven stations (IZVR, SCHL, SCTR, SLCR, TATR, TUDR, and VLDR) are located on much thicker sediments of Neogene origin, than station CFR which is located on Paleozoic sediments. The latter is more compact and with high seismic velocity up until surface; this is well reflected in the lower noise level observed in the microseismic domain. At larger periods (> 10 s), the higher noise levels are a consequence of the instrumentation and installation of the sensors.

The noise single station analysis, performed using the HVNR methodology, shows a distinct fundamental resonance peak at low frequencies for stations IZVR, SCHL, SCTR, SLCR, TATR, TUDR, VLDR. Its large amplitude and the absence of any azimuthal dependency are a strong indicator of the existence of a high-velocity contrast between the thick stack of sediments of about 3000 m and the bedrock at all these sites. This contrast is documented at 2600/3650 m/s near VLDR, and at 2800/3300 m/s at TUDR station (Raileanu, Annual report 2006). From Figs. 4 and 8 it can be observed that the resonance frequency of these stations increases from 0.15 to 0.28–0.29 Hz from the most southwestern station (TUDR) to the most north-eastern stations (TATR and VLDR). This increase is well correlated with the decrease of Neogene sediments from W to E from about 1300 m (near TUDR) to about 1000 m (near VLDR) (Raileanu, Annual report 2006).

For station CFR, the fundamental resonance frequency is observed at high frequency ($\sim$ 8 Hz) with an amplitude
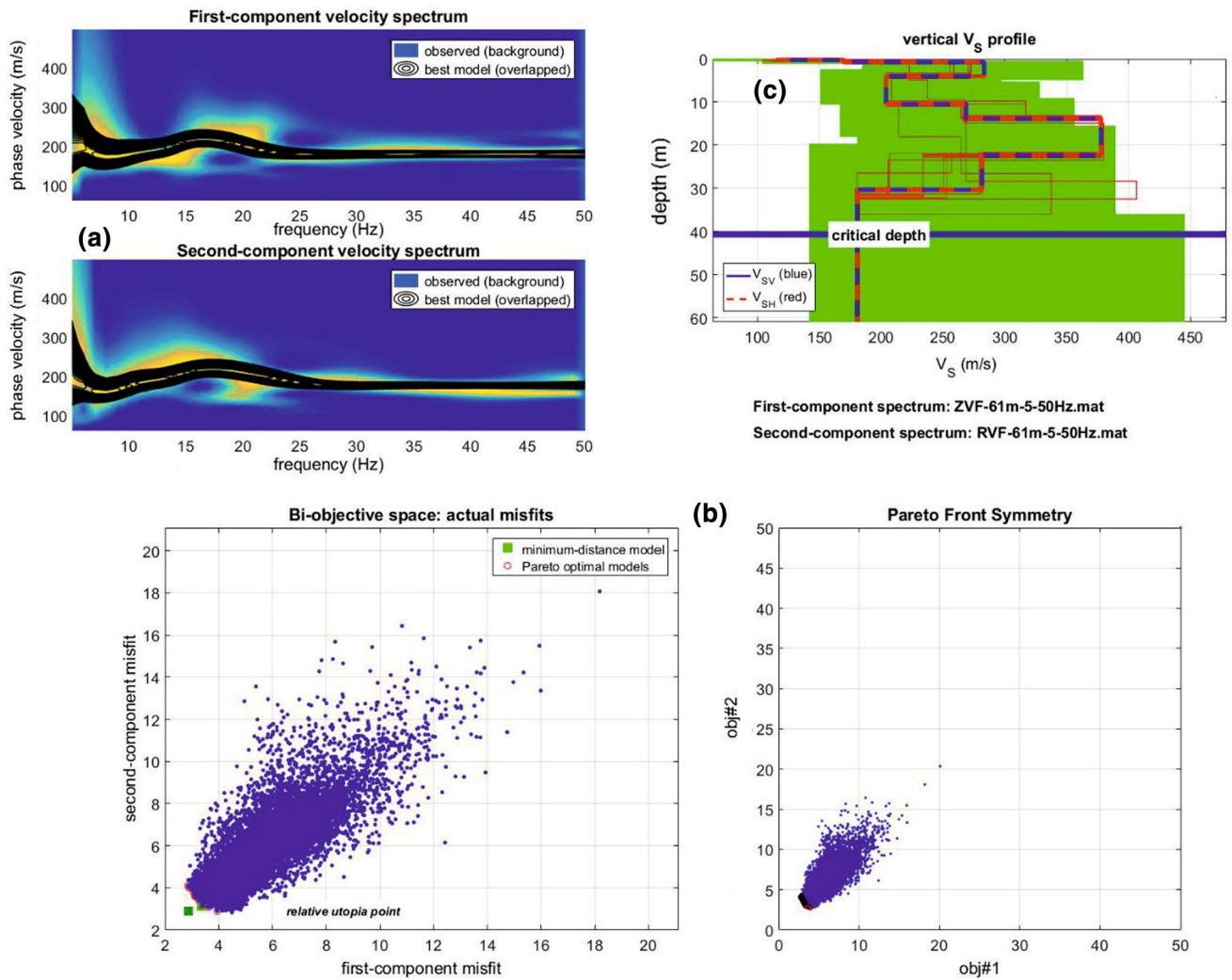
Fig. 13 **a** Joint analysis of the vertical and radial components (group velocities) of Rayleigh waves (colors in the background represent the field data while overlaying black contour lines represent the velocity spectra of the retrieved model) at station TATR. **b** Pareto front models of the joint inversion of vertical and radial components of Rayleigh wave. Distribution of the evaluated models in the bi-objective space (obj#1: vertical Rayleigh-wave misfit; obj#2: radial Rayleigh-wave misfit). **c** The retrieved vs profile

Table 1 Summary of the results obtained from HVNR analysis and inversion of the Rayleigh wave

Station	Computed Vs$_{30}$ (m/s)			Soil classification (EC 8)	Vs$_{30}$ (m/s) (EC 8)	Fundamental resonance	
	Vertical	Radial	Joint inversion			Frequency (Hz)	Amplitude
CFR	458	516	461	B	360–800	8.04	3.2
IZVR	233	240	252	C	180–360	0.19	5.2
SCHL	239	297	301	C	180–360	0.22	3.9
SCTR	207	190	227	C	180–360	0.24	5.0
SLCR	–	–	–	–	–	0.19	5.1
TATR	267	239	263	C	180–360	0.29	4.5
TUDR	239	276	214	C	180–360	0.15	6.4
VLDR	282	261	274	C	180–360	0.28	5.1

not larger than 3. At this station, the basement is placed at 1200 m depth, but the velocity contrast is very low, from 3400 to 3500 m/s.

Also, for this station, a strong dependency on the azimuth of the resonance amplitude is noticed. This suggests a complex site effect due most probably to the surface rock degradation and topographical irregularities observed at the site.

In the absence of a reference site, we applied a similar technique with HVNR method to earthquake data to investigate the site amplification. The HVSR technique provided consistent results in all sites. For the stations IZVR, SCHL, SCTR, SLCR, TATR, TUDR, VLDR amplifications were identified for a wide frequency band, from 0.15 Hz to 5–7 Hz. The fundamental resonance frequency obtained from noise data is present also in all HVSR curves, but only for station VLDR dominates the spectral ratio. If we look at the HVNR results for this station (Fig. 9), we can observe that the fundamental resonance peak has the largest amplitude and is the narrowest of all HVNR curves. This suggests a strong velocity contrast between sediments and bedrock which is also transmitted to the earthquake ground motion. For station CFR, the HVSR and HVNR curves are in good agreement, with no amplification till 2–4 Hz and an increase of the amplification up to 10 Hz. In case of HVSR, the maximum amplitude reaches three between 8 and 10 Hz.

Finally, using active seismic data (Rayleigh waves) generated by vertical force, it was possible to retrieve surface shear-wave velocity profiles, and then to calculate Vs_{30} values and propose the soil class for each site according to EC8 soil classes. For each station, we used three types of datasets for inversion: Rayleigh wave data recorded on the vertical and radial components and the combined dataset of the first two. The inversions of these data provided slightly different velocity profiles and Vs_{30} values (Table 1), but the soil class deduced no matter what dataset we used in the inversion was the same at each station. However, we strongly recommend the joint inversion of multiple datasets (Rayleigh and Love waves, Radial-to-Vertical Spectral Ratio—RVSR) to better constrain the final solution.

Compliance with ethical standards

Conflict of interest On behalf of all authors, the corresponding author states that there is no conflict of interest.

References

Balan SF, Ioane D, Cioflan C, Panea I, Apostol B, Malita Z, Chitea F, Anghelache MA (2014) Scenarios for local seismic effects of Tulcea (Romania) crustal earthquakes—preliminary approach of the seismic risk characterization for Tulcea city. In: Bostenaru D, Armas M, Goretti A (eds) Earthquake hazard impact and urban planning. Springer, Dordrecht, pp 85–103

Bard PY (1999) Microtremor measurements: a tool for site effects estimation. In: Irikura K, Kudo K, Okada H, Sasatani T (eds) The effects of surface geology on seismic motion. Balkema, Rotterdam, pp 1251–1279

Dal Moro G (2008) VS and VP vertical profiling and poisson ratio estimation via joint inversion of Rayleigh waves and refraction travel times by means of bi-objective evolutionary algorithm. J Appl Geophys 66:15–24

Dal Moro G (2014) Surface wave analysis for near surface applications. Elsevier, Amsterdam, p 244

Dal Moro G, Ferigo F (2011) Joint analysis of Rayleigh and love wave dispersion for near-surface studies: issues, criteria and improvements. J Appl Geophys 75:573–589

Dal Moro G, Pipan M, Gabrielli P (2007) Rayleigh wave dispersion curve inversion via genetic algorithms and marginal posterior probability density estimation. J Appl Geophys 61(1):39–55

Diaz J, Villasenor A, Morales J, Pazos A, Cordoba D, Pulgar J, Garcia-Lobon JL, Harnafi M, Carbonell R, Gallart J, TopoIberia Seismic Working Group (2010) Background noise characteristics at the IberArray Broadband Seismic Network. Bull Seismol Soc Am 100(2):618–628

Evangelidis CP, Melis NS (2012) Ambient noise levels in Greece as recorded at the Hellenic Unified Seismic Network. Bull Seismol Soc Am 102(6):2507–2517

Field EH, Jacob KH (1995) A comparison and test of various site-response estimation techniques, including three that are not reference-site dependent. Bull Seismol Soc Am 85(4):1127–1143

Ghica DV, Grecu B, Popa M, Radulian M (2016) Identification of blasting sources in the Dobrogea seismogenic region, Romania using seismo-acoustic signals. Phys Chem Earth Parts A/B/C 95:125–134

Grecu B, Raileanu V, Bala A, Tataru D (2011) Estimation of site effects in the eastern part of Romania on the basis of H/V ratios of S and coda waves generated by Vrancea intermediate-depth earthquakes. Rom J Phys 56:563–577

Grecu B, Neagoe C, Tataru D (2012) Seismic noise characteristics at the Romanian broadband seismic network. J Earthq Eng 16(5):644–661

Grecu B, Negoe C, Tataru D, Borleanu F, Zaharia B (2016) Analysis of seismic noise in the Romanian-Bulgarian cross-border region (submitted to Journal of Seismology)

Grecu B, Neagoe C, Partheniu R, Nastase E, Zaharia B (2017) New seismic noise model for Romania, science and technologies in geology, exploration and mining. In: Proceedings of 17th International Multidisciplinary Scientific Geoconference, pp 285–292, Eds. STEF92 Technology Ltd (**ISBN 976-619-7408-00-3**)

Ibs-von Seht M, Wohlenberg J (1999) Microtremor measurements used to map thickness of soft sediments. Bull Seis Soc Am 89(1):250–259

Ionesi L (1989) Geologia Romaniei: unitati de platforma si orogenul Nord Dobrogean (translated title: The geology of Romania: platform units and the North-Dobrogean orogen). Thesis, Univ. Al. I. Cuza, Iasi, Romania. p 253 (**in Romanian**)

Konno K, Ohmachi T (1998) Ground-motion characteristics estimated from spectral ratio between horizontal and vertical components. Bull Seis Soc Am. 88(1):228–241

Lermo J, Chávez-García FJ (1993) Site effect evaluation using spectral ratios with only one station. Bull Seismol Soc Am 83(5):1574–1594

Matenco L, Bertotti G, Cloetingh S, Dinu C (2003) Subsidence analysis and tectonic evolution of the external Carpathian-Moesian Platform region during Neogene times. Sed Geol 156:71–94

McNamara DE, Buland RP (2004) Ambient noise levels in the continental United States. Bull Seis Soc Am 94:1517–1527

Nakamura Y (1989) A method for dynamic characteristics estimation of subsurface using microtremor on the ground surface. QR Railw Tech Res Inst 30:25–33

Oncescu MC, Marza V, Rizescu M, Popa M (1999) The Romanian earthquakes catalogue between 984 and 1997. In: Wenzel F, Lungu D (eds) Vrancea earthquakes: tectonics, hazard and risk mitigation. Kluwer Academic Publishers, Berlin, pp 43–47

Peterson J (1993) Observation and modeling of seismic background noise, U.S. Geol. Surv. Tech. Rept. 93–322, pp 1–95

Philips WS, Aki K (1986) Site amplification of coda waves from local earthquakes in central California. Bull Seism Soc Am 76:627–648

Popa M, Oros E, Dinu C, Radulian M, Borleanu F, Rogozea M, Munteanu I, Neagoe C (2016) The 2013 earthquake swarm in the galati area: first results for a seismotectonic interpretation. In: Vacareanu R, Ionescu C (eds) The 1940 Vrancea Earthquake. issues, insights and lessons learnt. Springer International Publishing, Switzerland. https://doi.org/10.1007/978-3-319-29844-3_17

Radulian M, Mandrescu N, Panza GF, Popescu E, Utale A (2000) Characterization of seismogenic zones of Romania. In: Panza G, Radulian M, Trifu C (eds) Seismic hazard of the Circum-Pannonian Region. Birkhäuser, Basel, pp 57–77

Raileanu V (2006) Annual report for the Contract no: 31 N/23.01.2006, Project—Advanced research of the disaster management of the strong Romanian earthquakes, Director of the project dr. Raileanu V., NIEP

Sandulescu M (ed) (1984) Geotectonica Romaniei (translated title: Geotectonics of Romania). Tehnica, Bucharest, p 335 (in Romanian)

Site Effects Assessment using Ambient Excitations (SESAME) European project (2005) Deliverable D23.12—Guidelines for the implementation of the H/V spectral ratio technique on ambient vibrations: measurements, processing and interpretation. http://www.sesame-fp5.obs.ujf-grenoble.fr

Stutzmann E, Schimmel M, Patau G, Maggi A (2009) Global climate imprint on seismic noise. Geochem Geophys Geosyst. https://doi.org/10.1029/2009GC002619